Dimitrios Krikorian[1]
Athanassios Stavrakoudis[1]
Nikolaos Biris[1]
Constantinos Sakarellos[1]
David Andreu[2]
Eliandre de Oliveira[2*]
Gábor Mezö[3]
Zsuzsa Majer[4]
Ferenc Hudecz[3,4]
Sytske Welling-Wester[5]
Manh Thong Cung[6]
Vassilios Tsikaris[1]

[1] *Department of Chemistry, Section of Organic Chemistry and Biochemistry, University of Ioannina, 45110 Ioannina, Greece*

[2] *Department of Experimental and Health Sciences, Universitat Pompeu Fabra, 08003 Barcelona, Spain*

[3] *Research Group of Peptide Chemistry, Hungarian Academy of Sciences, Budapest 112, P. O. Box 32, H-1518, Hungary*

[4] *Department of Organic Chemistry, Eötvös L. University, Budapest, Hungary*

[5] *Department of Medicinal Microbiology, University of Groningen, Groningen, The Netherlands*

[6] *Laboratoire de Chimie Physique Macromoléculaire, UMR 7568 CNRS—INPL, Groupe ENSIC, 1 rue Grandville, B. P. 451, 54001 Nancy Cedex, France*

Influence of Sequential Oligopeptide Carriers on the Bioactive Structure of Conjugated Epitopes: Comparative Study of the Conformation of a *Herpes simplex* Virus Glycoprotein gD-1 Epitope in the Free and Conjugated Form, and Protein "Built-In" Crystal Structure

Received 12 December 2005; revised 2 February 2006; accepted 14 February 2006
Published online 21 February 2006 in Wiley InterScience (www.interscience.wiley.com). DOI 10.1002/bip.20486

Abstract: *Synthetic carriers play an important role in immunogen presentation, due to their ability of inducing improved and specific responses to conjugated epitopes. Their influence on the bioactive conformation of the epitope, though admittedly crucial for relevant in vitro and in vivo applications, is difficult to evaluate, given the usual lack of information on the complex conformational*

Correspondence to: Vassilios Tsikaris, e-mail: btsikari@cc.uoi.gr
Contract grant sponsor: COST Chemistry Action and Hungarian National Science Fund (HNSF)
Contract grant number: D13/0007/00 (COST); OTKA T 043576 and T 049814 (HNSF)
Present address: Proteomics Unit, Barcelona Science Park, 08028 Barcelona, Spain

features determined by the nature of the carrier and the mode of ligation. Using the Herpes simplex *virus glycoprotein D-1 epitope (Leu^{9}–Lys–Nle–Ala–Asp–Pro–Asn–Arg–Phe–Arg–Gly–Lys–Asp–Leu^{22}) as a model, we have performed a detailed conformational analysis on the free epitope peptide in solution and on three constructs in which the epitope was conjugated to sequential oligopeptide carriers {Ac–[Lys–Aib–Gly]$_4$–OH (SOC$_4$)} (through either a thioether or an amide bond; Ac: acetyl) and polytuftsin oligomers {H–[Thr–Lys–Pro–Lys–Gly]$_4$–NH$_2$ (T20)}, (through a thioether bond). The analysis of the epitope conformation in the parent protein, in carrier-conjugated and free form, suggests that the β-turn structure of the –Asp^{13}–Pro–Asn–Arg^{16}– segment is highly conserved and independent of the epitope form. However, small conformational variations were observed at the C-terminal part of the epitope, depending on the nature of the carrier.* © 2006 Wiley Periodicals, Inc. Biopolymers (Pept Sci) 84: 383–399, 2006

This article was originally published online as an accepted preprint. The ''Published Online'' date corresponds to the preprint version. You can request a copy of the preprint by emailing the Biopolymers editorial office at biopolymers@wiley.com

Keywords: *conformation of conjugated epitope peptides; glycoprotein D-1 epitope; sequential oligopeptide carriers; sequential oligopeptide carriers; tetratuftsin carrier; synthetic carriers; carrier-conjugated epitopes*

INTRODUCTION

The dissection of the antigenic properties of a protein down to selected segments of its primary structure and the use of such peptide segments as immunogens of predetermined specificity is a common and useful strategy in immunological studies. Frequently, these short peptides, though antigenic, are insufficiently immunogenic; however, their immunogenicity can be improved considerably by appropriate presentation through conjugation to either protein, oligopeptide, or other carriers.[1–11] Although peptide–carrier protein conjugates are routinely used for eliciting antipeptide antibodies in research contexts, their potential therapeutic (e.g., candidate vaccine) use is compromised by factors such as difficulties in standardizing the composition and structure of the conjugates, undesirable immune response to the carrier, etc. One possible alternative, conjugation of multiple copies of a peptide epitope to a synthetic carrier, leads to protein-like molecules of branched architecture and well-defined composition, with molecular weights up to 10 kD.[4,6,9] Such branched constructs have found numerous applications in immunology due to their contribution to overcoming the very low ability of short linear peptides to react specifically with antibodies or to induce an immune response.[10–25] These macromolecules can be relatively easily characterized and can also be designed to possess specific structural and functional properties. These advantages have placed the synthetic carrier approach at the center of extensive research activities.

Artificial carriers can adopt regular secondary structures that provide to conjugated epitopes the conformational freedom essential for optimal antibody recognition or for inducing antibodies able to recognize the cognate proteins.[5,9] The retention of the bioactive conformational state of the epitopes when conjugated to the carrier becomes a determining factor for relevant in vitro and in vivo applications. Nuclear magnetic resonance (NMR) studies in dimethylsulfoxide-d$_6$ (DMSO-d$_6$) solution of antigenic constructs based on a artificial sequential oligopeptide carrier (SOC$_n$) revealed that the epitopes, upon conjugation to the carrier, exhibited conformational features very similar to the epitope in the free state.[4,5,16] However, we are not aware of experimental data correlating the conformation of a peptide epitope in the free and conjugated state with the conformation of the corresponding sequence in the native protein structure.

In a previous work,[9] we reported on the effect of the structure and topology of the carrier macromolecule on antibody recognition of the *Herpes simplex* virus type 1 glycoprotein D (HSV gD-1) epitope H–Leu^{9}–Lys–Nle–Ala–Asp–Pro–Asn–Arg–Phe–Arg–Gly–Lys–Asp–Leu^{22}–NH$_2$, ([Nle^{11}]gD-9-22), where Nle replaces a native Met. This epitope was conjugated to the following synthetic and protein carriers: (i) the tetratuftsin carrier (H–[Thr–Lys–Pro–Lys–Gly]$_4$–NH$_2$, T20),[9,23] (ii) the sequential oligopeptide carrier (Ac–[Lys–Aib–Gly)$_4$–OH, SOC$_4$) (Ac: acetyl),[2,9] (iii) the polymeric branched-chain polypeptide (poly[Lys(Ser$_i$-DL-Ala$_m$)], SAK),[6,9] (iv) the tetrameric Lys-dendrimer construct (multiple antigenic peptide, MAP),[1,2,9] and (v) the widely used keyhole limpet hemocyanin (KLH) protein carrier. The conjugation of the epitope peptide to the carriers was realized through either thioether or amide bond. The results of binding experiments with the monoclonal antibody mAb A16 (a con-

formation-independent monoclonal antibody classified together with mAbs LP14, ID3 as a group VII monoclonal antibody of gD; Refs. 26 and 27), clearly indicated that the carrier-bound peptide epitope is recognized more efficiently than free peptide in all multivalent peptide conjugates except in the MAP and KLH conjugates. We found that the binding properties of conjugates vary 2.5–50-fold, depending on the carrier structure, the average degree of substitution, and on the binding assay used.[9]

The above results and the fact that the crystal structure of *H. simplex* virus glycoprotein D1 is available[28] prompted us to investigate the conformational features of the [Nle^{11}]gD-9-22 epitope in its free, conjugated, and protein ''built-in'' form relevant to antibody recognition. This investigation could contribute to understanding the propensity of artificial carriers to enhance the antigenicity and/or the immunogenicity of short linear peptides. Our knowledge regarding the recognition of the cognate protein by antibodies elicited against multiple epitope–carrier constructs could also be improved. Here we report on the circular dichroism (CD) and ^{1}H-NMR conformational analysis of [Nle^{11}]gD-9-22, both in the free and carrier- (SOC_4 and T20) conjugated form. These conjugates exhibited the highest binding for the mAb A16 compared to other conjugates studied.[9] Comparison with the crystal structure of the *Herpes simplex* virus glycoprotein D-1 reveals the presence of similar conformational characteristics in forms of the epitope peptide investigated.

MATERIALS AND METHODS

Peptides and Conjugates

Synthesis of the [Nle^{11}]gD-9-22 epitope [H–Leu^9–Lys–Nle–Ala–Asp–Pro–Asn–Arg–Phe–Arg–Gly–Lys–Asp–Leu^{22}–NH_2] (**1**) in free form, and its conjugation to SOC_4 through an amide bond (Ac-[SOC_4([Nle^{11}]gD-9-22)$_4$]) (**2**) has been previously reported.[9] Conjugation of the epitope to either SOC_4 (Ac-[SOC_4([Nle^{11}]gD-9-22-Cys)$_4$]) (**3**) or tetratuftsin (T20([Nle^{11}]gD-9-22-Cys)$_4$) (**4**) carriers through a thioether bond (Figure 1) required an analogue of [Nle^{11}]gD-9-22-Cys with an additional Cys residue at the C-terminus.[9]

Nuclear Magnetic Resonance

D_2O (99.8%) and tetradeutero 2,2,3,3-tetradeutero-3-(trimethylsilyl)-3-propionic acid sodium salt (TMPS-d_4) were purchased from Euriso-top (Gif-sur-Yvette, France). The free peptide or the conjugates were dissolved in H_2O/D_2O (95/5 v/v) (containing 0.02% sodium azide and TMPS-d_4 as an internal reference) at a 5 m*M* concentration of peptide epitope and the pH was adjusted to 4.0. Spectra were recorded at 4°C using a Bruker DRX600 NMR spectrometer. Two-dimensional (2D) total correlated spectroscopy (TOCSY) was performed on each compound with a mixing time, τ_m, of 70 ms. Four 2D nuclear Overhauser enhancement spectroscopy (NOESY) experiments with mixing times ranging from 100 to 500 ms were performed. The buildup curve[29] for different NOE correlations showed that spin diffusion was negligible for $\tau_m = 250$ ms. The spectral width in F1 was 6600 Hz. Water resonance suppression in the TOCSY and NOESY experiments was achieved using the water suppression by gradient-tailored excitation (WATERGATE) sequence.[30,31] Data processing was performed using the XWIN-NMR software. The peak intensities were extracted from the NOESY spectra ($\tau_m = 250$ ms) using the XEASY software[32] and the interproton distances were calculated taking as reference the distance of 1.78 Å between the two Asp–$C^{\beta}H_2$ protons.

CD Studies

CD studies of the Ac-[SOC_4([Nle^{11}]gD-9-22-Cys)$_4$] and T20([Nle^{11}]gD-9-22-Cys)$_4$ constructs were performed in aqueous solution, in a trifluoroethanol (TFE):water mixture (1:1, v/v) and in pure TFE. The spectra were recorded using a Roussel–Jobin dichrograph model VI (Jobin-Yvon, Longjumeau, France) in quartz cells with an optical path length of 0.02 cm at room temperature, under constant nitrogen flush. CD spectra were registered from $\lambda = 185$ nm to 270 nm. The concentration of the samples was 0.5–1.0 mg/mL. CD band intensities are expressed in mean residue ellipticity ($[\Theta]_{MR}$ in deg cm^2 dmol^{-1}). The CD conformational analysis of peptide 8–23 was reported previously.[33]

Structure Calculations

Structure calculations were carried out using the software CYANA (*c*ombined assignment and dynamics *a*lgorithm for *N*MR *a*pplications).[34,35] The distance restraints used as input in CYANA were derived from ^{1}H–^{1}H NOESY spectra of the peptides in aqueous solution at pH 4.0. Cross-peak intensities, classified as strong (up to 2.8 Å), medium (up to 3.5 Å), and weak (up to 5 Å) were used as restraints for the calculations. Appropriate corrections for center averaging were added to CYANA restraints for degenerate proton resonances (pseudo-atom) while no lower limits were used. Constraints for φ, ψ, and χ^1 angles were calculated using the HABAS program of the CYANA package. Coupling constants were included in one case (free epitope peptide) with a tolerance of 2.0 Hz. All distance and angle constraints were assigned with the default relative weight of 1. The default tolerance of 0.05 for the target function units was applied. Calculations were performed using the standard minimization protocol and the redundant dihedral angle constraints (REDAC) strategy implemented in CYANA. All peptides were modeled with an amide cap at the C-terminus. The norleucine and cysteine C-terminal residues in the peptide sequences were replaced by methionine in the modeling process (e.g., –Leu^9–Lys–Met–Ala–Asp–Pro–Asn–Arg–Phe–Arg–Gly–Lys–Asp–Leu^{22}–NH_2 or –Leu^9–Lys–Met–Ala–Asp–Pro–Asn–Arg–Phe–Arg–Gly–Lys–Asp–Leu^{22}–Met^{23}–NH_2). Graphical representation and figures were produced with the program MOLMOL.[36] The crystal

FIGURE 1 Schematic representation of conjugates of the *Herpes simplex* virus glycoprotein D-1 epitope peptide with sequential oligopeptide carriers SOC_4 and tetratuftsin (T20).

structure of the *Herpes simplex* virus glycoprotein D-1 bound to the human receptor HveA (PDB code: 1JMA), region –Leu[9]–Lys–Met–Ala–Asp–Pro–Asn–Arg–Phe–Arg–Gly–Lys–Asp–Leu[22]–, was used to compare the derived conformations.[28]

RESULTS AND DISCUSSION

^{1}H-NMR Analysis

H–Leu[9]–Lys–Nle–Ala–Asp–Pro–Asn–Arg–Phe–Arg–Gly–Lys–Asp–Leu[22]–NH$_2$. Figure 2 shows the NH region of the one-dimensional (1D) ^{1}H-NMR spectrum of peptide [Nle[11]]gD-9-22 in aqueous solution. Usually, in aqueous solutions, short linear peptides exhibit only a few and weak NOE connectivities even for long mixing times. However, in this case intense sequential NOE cross peaks were observed for the free peptide (Figure 3A). All the NOE data used for sequential assignment and structure determination of the peptide are summarized in Figure 4A. The large number of NOEs observed indicates the tendency of this short peptide to adopt a rather compact structure

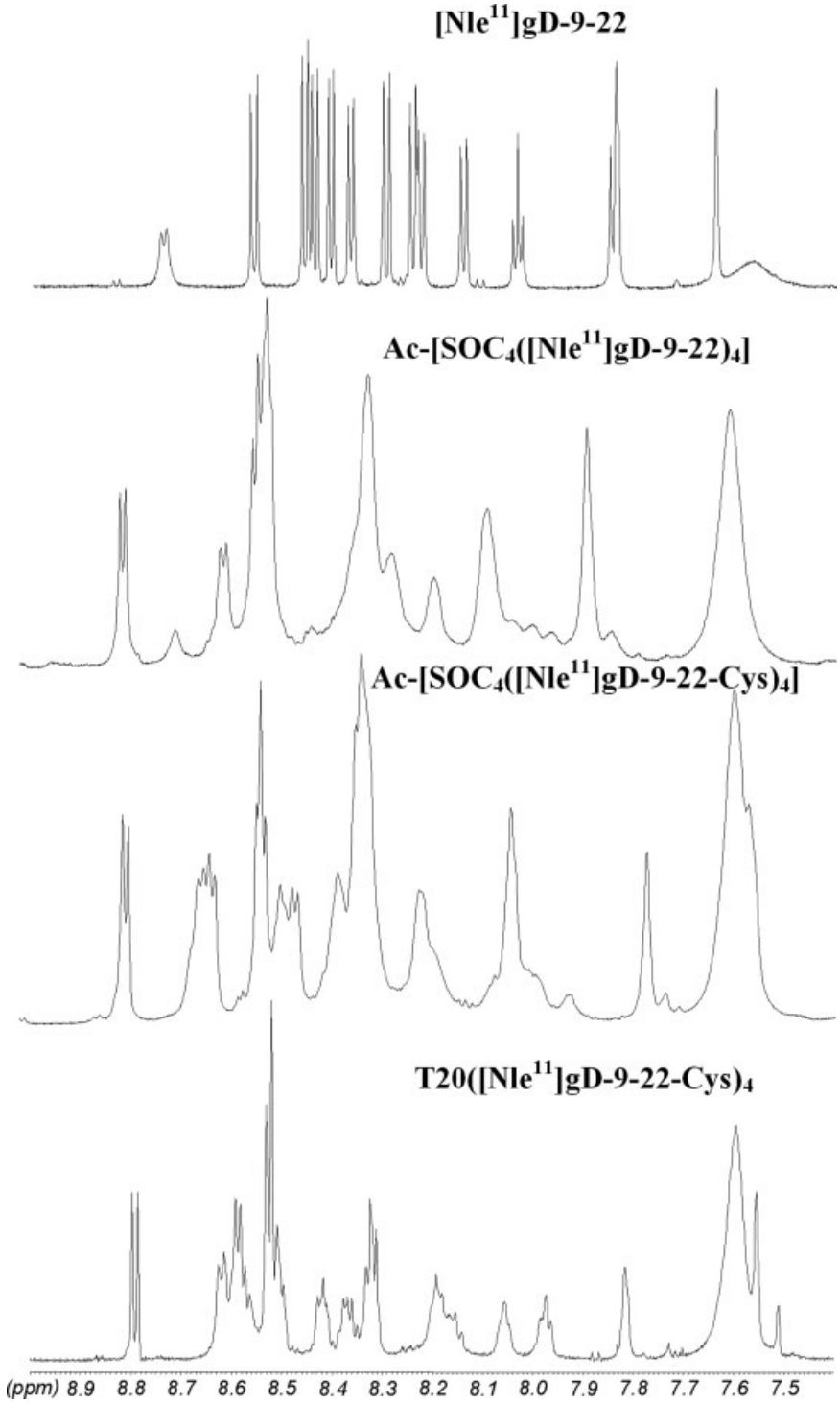

FIGURE 2 ^{1}H-NMR spectra of the free epitope peptide [Nle^{11}]gD-9-22, its conjugates with the SOC_4 carrier through an amide bond (Ac-[SOC_4([Nle^{11}]gD-9-22)$_4$]), with a SOC_4 carrier through a thioether bond (Ac-[SOC_4([Nle^{11}]gD-9-22-Cys)$_4$]), and with a T20 carrier through a thioether bond. Experimental conditions: 600.13 MHz 1D, solvent H_2O/D_2O (95/5 v/v), concentration 5 m*M* with regard to the epitope, pH $\sim$ 4.0, temperature 4°C.

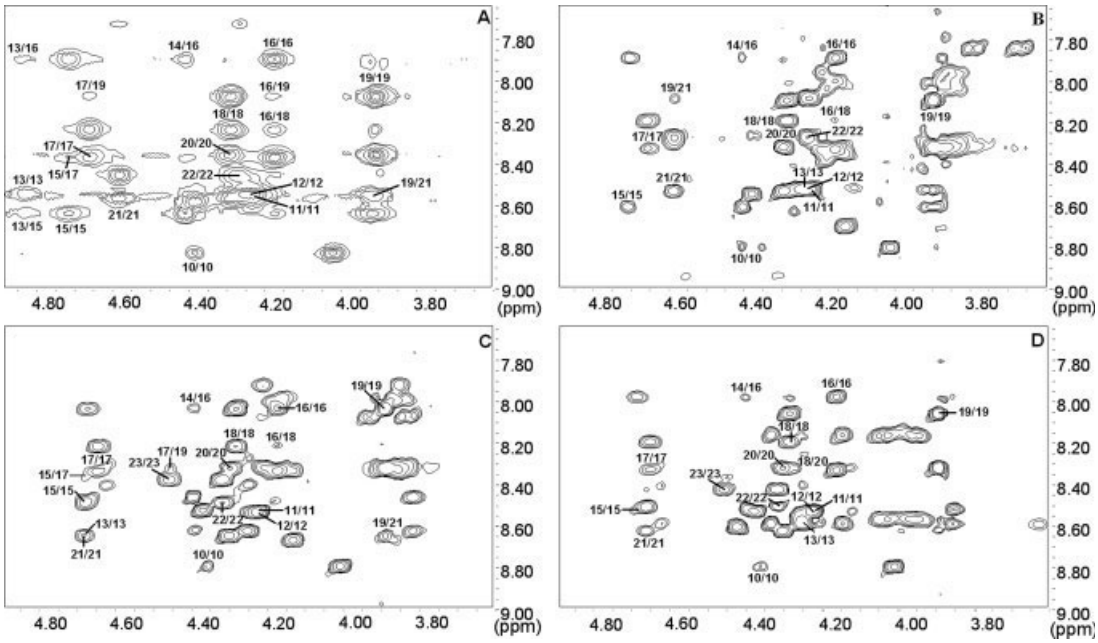

FIGURE 3 NH/C$^{\alpha}$H region of the 600.13-MHz NOESY spectra of the free epitope peptide [Nle^{11}]gD-9-22 (A), Ac-[SOC$_4$([Nle^{11}]gD-9-22)$_4$] (B), Ac-[SOC$_4$([Nle^{11}]gD-9-22-Cys)$_4$] (C), and T20([Nle^{11}]gD-9-22-Cys)$_4$ (D), in H_2O/D_2O (95/5, v/v), pH $\sim$ 4, temperature 4° C, mixing time 250 ms. The assignment of selected NOEs is shown.

even in water. The detection of almost all the expected NOE types $d_{\alpha N}(i, i + 2)$, $d_{NN}(i, i + 2)$, and $d_{\alpha N}(i, i + 3)$ in the segment –Asp^{13}–Pro–Asn–Arg–Phe–Arg–Gly–Lys–Asp^{21}– suggests the presence of a 3_{10}-helix structure in this part of the molecule.[37] Although the 3_{10}-helix is less stable than the α-helix and considered unlikely for long peptide stretches,[38] the presence of oppositely charged side chains at positions i and $i + 3$ (Asp^{13}/Arg^{16} and Arg^{18}/Asp^{21}) of the helix probably favors, through side-chain–side-chain ionic interactions, the stabilization of the 3_{10}-helix (see also the section on structure calculation below). It is worth mentioning here that the number of NOEs observed in our case is considerably higher than those reported previously for the same segment as either εAhx–Pro–Ser–Leu^{9}–Lys–Met–Ala–Asp–Pro–Asn–Arg–Phe–Arg–Gly–Lys–Asp–Leu^{22}–Pro–εAhx (Ref. 39; εAhx: ε-aminohexanoic acid) or εAhx–Met^{11} Ala–Asp–Pro–Asn–Arg–Phe–Arg–Gly–Lys–Asp–Leu^{22}–Pro–Val–Leu–Asp–Gln–Leu–Thr–Asp–Pro–Pro–εAhx (Ref. 40) derivatives in aqueous solution at room temperature. These differences may arise either from the different experimental conditions (temperature, pH, etc.) or from peptide elongation at the C-terminal part. Interestingly, the C-terminal part of the epitope exhibits an extended conformation within the native protein sequence.[28] Nevertheless, all studies agree with the presence of a type I/III β-turn in the –Asp^{13}–Pro–Asn–Arg^{16}– segment. This is consistent with the low absolute temperature coefficient value of the Arg^{16}–NH proton (-3.0×10^{-3} ppm/K) and the observed NOE effects (Pro^{14}–C$^{\alpha}$H/Arg^{16}–NH, Asn^{15}–NH/Arg^{16}–NH, Pro^{14}–C$^{\alpha}$H/Phe^{17}–NH).[37] Finally, the absence of medium-range NOE effects at the N-terminal end denotes a higher flexibility of this segment of the molecule.

H–Leu^{9}–Lys–Nle–Ala–Asp–Pro–Asn–Arg–Phe–Arg–Gly–Lys–Asp–Leu^{22}– conjugated to Ac–(Lys–Aib–Gly)$_4$–OH Carrier. In this compound the epitope was conjugated to the carrier through an amide bond between Lys–N$^{\varepsilon}$H$_2$ of the carrier and the C-teminal carboxylic group of the epitope peptide (Figure 1). The concentration of the construct used for the NMR experiments was calculated with regard to the epitope. Therefore the concentration of the carrier is about four times lower as compared to that of the epitope. The proton assignment of the epitope was made by the combined use of TOCSY and NOESY experiments. Comparison with the free peptide facilitated and confirmed the assignment. It is important to note here that the chemically equivalent protons of the four copies of the epitope appeared as a single resonance (Figure 2). This fact facilitates the proton NMR analysis and indicates that the epitope copies do not interact with each other or with the carrier because otherwise multiple resonances would be

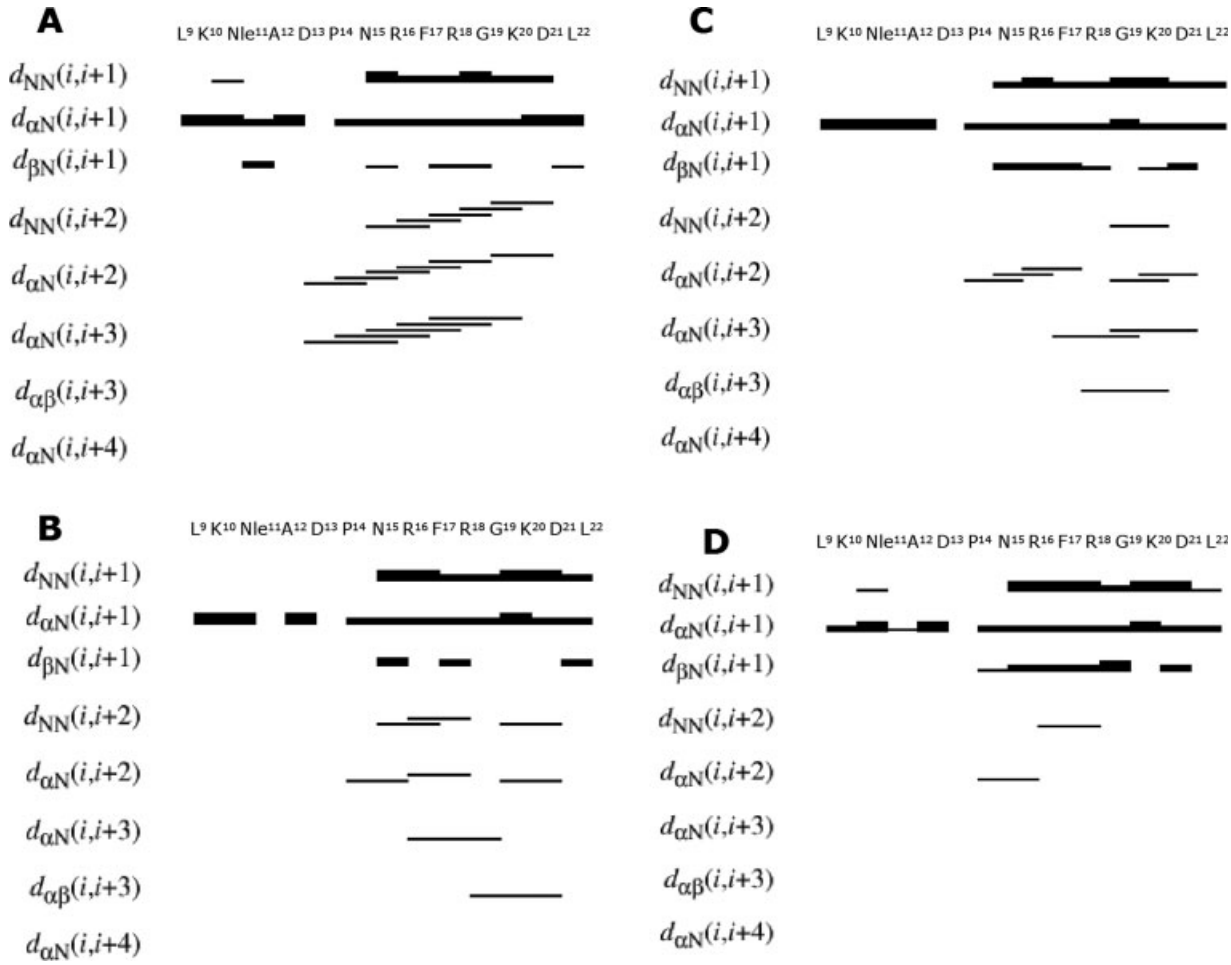

FIGURE 4 Overview of NOE connectivities of the free epitope peptide [Nle[11]]gD-9-22 (A), Ac-[SOC_4([Nle[11]]gD-9-22)$_4$] (B), Ac-[SOC_4([Nle[11]]gD-9-22-Cys)$_4$] (C), and of T20([Nle[11]]gD-9-22-Cys)$_4$ (D). The relative intensities of each filled bar indicates the strength of the NOE constraints.

expected. In addition, as it has been previously demonstrated, each amide proton of the Ac–(Lys–Aib–Gly)$_4$–OH carrier appears as separate resonances despite the fact that it is formed by the repetitive sequence –Lys–Aib–Gly–. This behavior was attributed to the helical structure of the carrier.[3] The fact that NH signals of the SOC_4 carrier are of very low intensities in the case of Ac-[SOC_4([Nle[11]]gD-9-22)$_4$] confirms the above suppositions (Figure 2).

Figures 3B and 4B show the detected NOE effects for the SOC_4-conjugated epitope peptide. The conjugated epitope exhibits a similar NOE pattern with that of the free peptide, especially in the central part of the molecule. Some of the nonassigned NOEs (Figures 3B) originate from the carrier backbone protons for which the sequential assignment cannot be performed under these experimental conditions. Although the expected $d_{\alpha N}(i, i + 2)$, $d_{NN}(i, i + 2)$, and $d_{\alpha N}(i, i + 3)$ NOE effects for the –Asp[13]–Pro–Asn–Arg–Phe–Arg–Gly–Lys–Asp[21]– segment in the case of Ac-[SOC_4([Nle[11]]gD-9-22)$_4$] were not fully resolved, it is evident from the assigned NOE effects that this conjugate has common conformational features with the free peptide. The NOE effects observed in the –Asp[13]–Pro–Asn–Arg[16]– segment (Asn[15]–NH/Arg[16]–NH, Pro[14]–C$^{\alpha}$H/Arg[16]–NH) are in agreement with the presence of type I/III β-turn structure. Moreover, the structure similarity in the central part of the epitope peptide in its free and SOC_4-conjugated form is further supported by the fact that the chemical shift values of the NH and C$^{\alpha}$H backbone protons exhibit only very small differences (Figure 5A). An exception to this trend was the difference observed for the chemical shift of the Asp[13]–C$^{\alpha}$H proton, which appeared strongly upfield shifted in the conjugated form of the epitope. This shifting could be explained

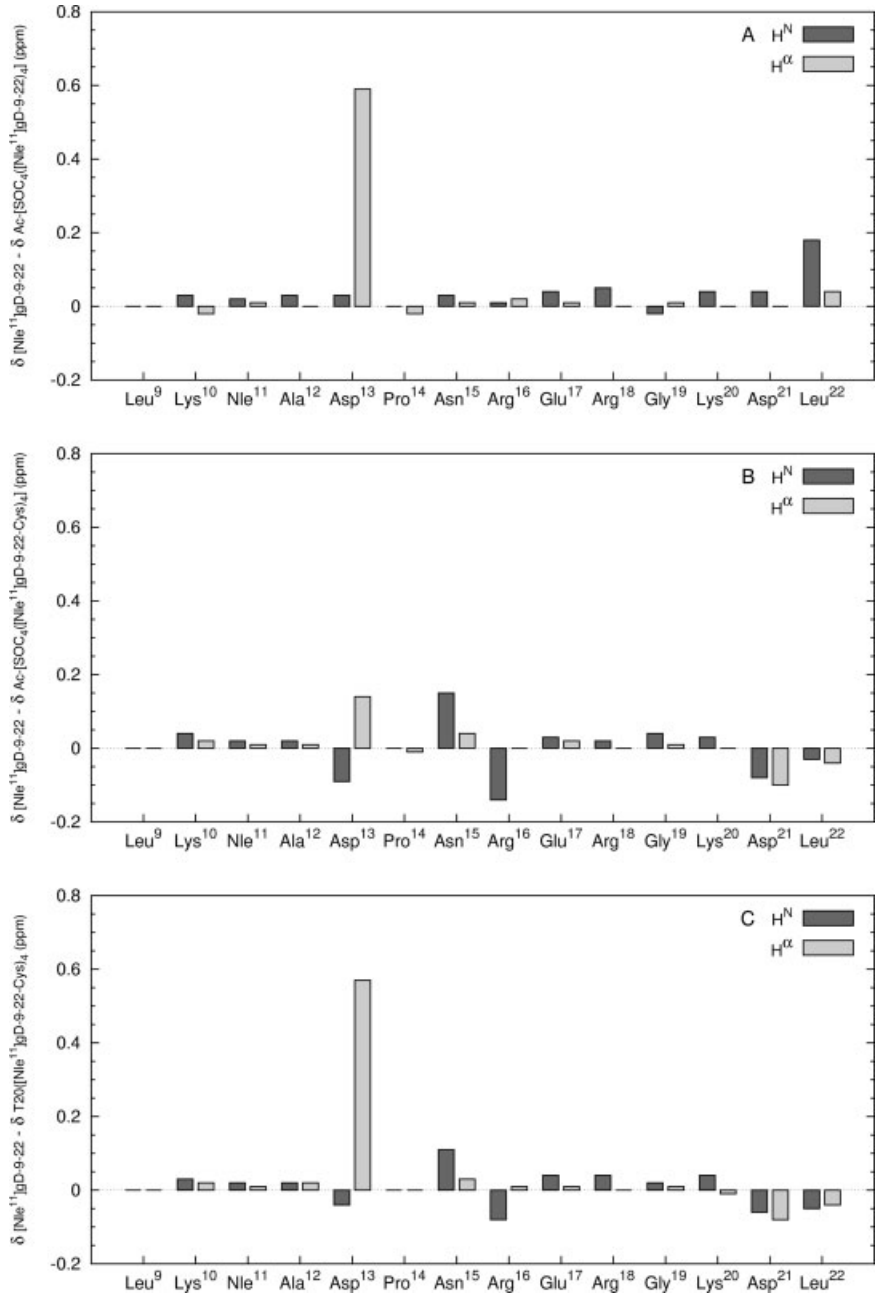

FIGURE 5 Perturbations of the proton resonances of the *Herpes simplex* virus glycoprotein D-1 epitope [Nle^{11}]gD-9-22 conjugated to Ac–(Lys–Aib–Gly)$_4$–OH (A), [Nle^{11}]gD-9-22-Cys conjugated to Ac–(Lys–Aib–Gly)$_4$–OH (B), and [Nle^{11}]gD-9-22-Cys conjugated to H–[Thr–Lys–Pro–Lys–Gly]$_4$–NH_2 (C) carriers with reference to free peptide.

by an alteration of the vicinal φ and/or ψ dihedral angle values in the conjugated form.[41,42] These variations influence the chemical shift value of the Asp^{13}–$C^\alpha H$ proton, because they determine the relative orientation of the adjacent carbonyl groups and the distance between the H^α and O atoms. In turn, the magnetic anisotropy of the carbonyl bond is expected to influence the chemical shift value of H^α. From the CYANA calculations (see discussion below), it is concluded that the ψ angle of Asp^{13} changes from 162° in the free form to 120° in the conjugated form while the φ angle value remains almost invariable. Finally, the difference observed for the Leu^{22}–NH chemical shift between the free and SOC_4-conjugated states of the epitope must be attributed to the changes induced in this part of the molecule upon conjugation.

H–Leu^{9}–Lys–Nle–Ala–Asp–Pro–Asn–Arg–Phe–Arg–Gly–Lys–Asp–Leu^{22}–Cys–NH$_2$ Conjugated (Through Thioether) to Ac–(Lys–Aib–Gly)$_4$–OH Carrier. In this conjugate epitope, peptides were coupled with the carrier by using thioether bond (Figure 1). As observed in the previous case, the chemically equivalent protons of the four epitope copies give rise to a single resonance. The total number and the intensity of the NOE effects detected for the epitope of this compound are comparable to those observed for the free peptide (Figures 3C and 4C). The β-turn structure in the –Asp^{13}–Pro–Asn–Arg^{16}– segment is also present in this conjugate as revealed by the observed NOE effects (Asn^{15}–NH/Arg^{16}–NH, Pro^{14}–C$^{\alpha}$H/Arg^{16}–NH). Comparison of the chemical shift values of the NH and C$^{\alpha}$H backbone protons between the free and carrier-conjugated forms of the epitope indicates some differences in the β-turn sequence (–Asp^{13}–Pro–Asn–Arg^{16}–) (Figure 5B). The Asp^{13}–C$^{\alpha}$H proton is again, though to a less extent, upfield shifted in the conjugated form compared to the free epitope peptide. Interestingly, the chemical shift values of the Asn^{15}–NH and Arg^{16}–H protons change when compared to the free epitope peptide (Figure 5B). Because the differences in the chemical shift values of the rest backbone protons are not significant (Figure 5B), the observed variations for the $i + 2$ and $i + 3$ (Asn^{15} and Arg^{16}) residues of the β-turn may reflect either the disappearance of the β-turn or a shifting of the conformational equilibrium between type I and III β-turns. The β-turn transition is the most probable reason for the Asn^{15}–NH and Arg^{16}–NH chemical shift variations because the detected NOE effects in the –Asp^{13}–Pro–Asn–Arg^{16}– segment are very similar in both cases. This supposition is supported by the structure calculations results (see discussion below), which provide evidence for the presence of a β-turn close to type III in the conjugated epitope instead of a type I β-turn in the free peptide. It is worth mentioning here that the difference between the type I and III β-turn is very small and refers only to φ and ψ values of the $i + 2$ residue of the turn (the ideal type I β-turn has $\varphi = -60^{\circ}$, $\psi = -30^{\circ}$; and $\varphi = -90^{\circ}$, $\psi = 0^{\circ}$ for the $i + 1$ and $i + 2$ residues, respectively, while type III β-turn has $\varphi = -60^{\circ}$, $\psi = -30^{\circ}$; and $\varphi = -60^{\circ}$, $\psi = 30^{\circ}$ for the $i + 1$ and $i + 2$ residues, respectively[43]). A clear distinction between the two types of turns cannot be estimated by ^{1}H-NMR spectroscopy.

H–Leu^{9}–Lys–Nle–Ala–Asp–Pro–Asn–Arg–Phe–Arg–Gly–Lys–Asp–Leu^{22}–Cys–NH$_2$ Conjugated (Through Thioether) to Oligotuftsin (H–[Thr–Lys–Pro–Lys–Gly]$_4$–NH$_2$) Carrier. In this conjugate, epitope peptides were conjugated with the carrier by thioether linkage (Figure 1). Chemicaly equivalent amide protons of all four copies of the epitope in the T20 conjugate give rise to a single ^{1}H-NMR signal. This suggest that despite the fact that T20 exhibits characteristics of random coil conformation,[23] the spacial orientation of the conjugated epitope peptides does not allow the interaction between them or with the carrier. In addition, the pattern of the NOE effects in the central part of the epitope resembles to that observed for the same sequence in the free form (Figures 3D and 4D). The detected NOE effects Asn^{15}–NH/Arg^{16}–NH, Pro^{14}–C$^{\alpha}$H/Arg^{16}–NH in the –Asp^{13}–Pro–Asn–Arg^{16}– segment reveal that the β-turn structure is also conserved in this epitope conjugate (Figure 3D). The absence of type $d_{\alpha N}(i, i + 2)$, $d_{NN}(i, i + 2)$, and $d_{\alpha N}(i, i + 3)$, NOE signals in the C-terminal part of the epitope denotes a rather high flexibility of this segment. This flexibility is probably potentiated by the carrier, which due to its random conformation permits a higher mobility to the conjugated epitope.

The differences in the chemical shift values of the NH and C$^{\alpha}$H backbone protons of the conjugated epitope when compared to those of the free form are shown in Figure 5C. The shifting of the conformational equilibrium toward type III β-turn in the conjugated form is probably responsible for the observed differences of the chemical shift values of the Asn^{15} and Arg^{16} amide protons (see discussion below). In agreement with the preceding cases, the variation of the Asp^{13}–C$^{\alpha}$H proton chemical shift value (Figure 5C) could be explained by the ψ dihedral angle changes of Asp^{13} (from 162° in the free state change to 120° in the conjugated form).

CD Analysis

CD conformational studies of the free H–Ser^{8}–Leu–Lys–Met–Ala–Asp–Pro–Asn–Arg–Phe–Arg–Gly–Lys–Asp–Leu–Pro^{23}–NH$_2$ epitope were previously reported.[33] The CD spectra of the free [Nle]gD-9-22-Cys epitope peptide used for conjugation with sequential carriers were not different from those reported earlier for the 8–23 epitope peptide (data not shown). Namely, the CD spectrum suggested the presence of both unordered conformation and turn elements in water. When the TFE content in the TFE–water solvent mixture was increased, the ordered conformation corresponding to 3_{10}-helix and/or turn structures was predominant.[33] The CD spectra of the free [Nle]gD-9-22-Cys epitope peptide used for conjugation with sequential carriers were not different from those reported earlier for 8–23 epitope peptide (data not shown). CD studies of the Ac-[SOC$_4$([Nle^{11}]gD-9-22-Cys)$_4$] and

T20([Nle^{11}]gD-9-22-Cys)$_4$ constructs were performed in aqueous solution, in a TFE:water mixture (1:1, v/v), and in TFE. The CD spectra of both constructs recorded in these solvents showed only small differences. It is interesting to note that the tetratuftsin derivative adopted a highly unordered conformation even in TFE,[23] while the SOC_4 carrier a 3_{10}-helix structure.[18] In water, both conjugates showed rather unordered structures characterized by spectra containing a negative maximum at $\lambda = 199$ nm with a shoulder at $\lambda =$ 226–227 nm corresponding to $\pi\pi^*$ and $n\pi^*$ transitions, respectively. According to θ values, the SOC_4 conjugate has slightly higher helicity. ($\theta_{199} = -7.3 \cdot 10^3$ and $\theta_{226} = -1.4 \cdot 10^3$ for SOC_4 conjugate and $\theta_{199} = -8.9 \cdot 10^3$ and $\theta_{227} = -1.1 \cdot 10^3$ for the T20 conjugate were detected.) The differences observed between ^{1}H-NMR and CD results regarding the helix content in aqueous solution may rise to some extent from the different experimental conditions (e.g., CD and ^{1}H-NMR spectra were recorded at room temperature and 4°C, respectively). The helix content considerably increases upon addition of TFE, resulting in spectra typical for helical conformations in TFE (a positive band at $\lambda =$ 192 nm and two negative at $\lambda = 208$ and 222 nm, respectively). In TFE, the spectra of the two conjugates were almost identical ($\theta_{192} = 3.8 \cdot 10^3$, $\theta_{208} = -4.7 \cdot 10^3$, and $\theta_{222} = -3.3 \cdot 10^3$ for the SOC_4 conjugate; $\theta_{192} = 3.8 \cdot 10^3$, $\theta_{208} = -5.1 \cdot 10^3$, and $\theta_{222} = -3.6 \cdot 10^3$ for T20 conjugate). The θ values (low intensities) suggested that the spectra referred rather to 3_{10}-helix than to α-helical structure. The 3_{10}-helix structure consists of repeated structure elements of type III β-turn,[44,45] which is in agreement with the NMR results. It is worth mentioning that these spectra were almost identical with the ones measured for the free epitope peptide (data not shown). Based on CD data described above, we conclude that the pattern of the CD spectra of the conjugates studied is dominated by the spectral features characteristic for the free epitope peptide. Consequently, it seems rational to speculate that the conformation of both conjugates is dominated by the covalently attached epitope peptide. However, minor differences in the CD spectra of conjugates suggest that the SOC_4 conjugate has slightly more ordered structure, while the T20 conjugate shows more flexibility. These findings are essentially in agreement with the NMR derived structure of the free and carrier-conjugated epitope.

Structure Calculations

The structure of the [Nle^{11}]gD-9-22 epitope in its free and conjugated forms was calculated on the basis of distance and dihedral angle restraints (Table I), using the CYANA software. The Met residue has been used for the CYANA structure calculations instead of Nle^{11} and Cys^{23}. For each molecule, 100 structures were generated, and the 10 best ones were selected on the basis of their target functions and minimal number of restraint violations. After the first run of CYANA, without hydrogen-bonding restraints, hydrogen bonds assumed present (i.e., if H · · · O distance was less than 2.5 Å and N · · · H · · · O angle value was >145°) in at least 7 out of the 10 best structures were inserted as additional restraints to a new CYANA run. These restraints were taken into consideration for further CYANA runs if they had no impact on other (experimentally determined) initial restraints. The procedure was repeated until no other restraints came out. The φ and φ values for the averaged structures calculated from the 10 lowest target function structures for all the compounds studied in this work are listed in Table II and plotted in Figure 6. For comparison, the φ and ψ dihedral angle values of the –Leu^9–Lys–Met–Ala–Asp–Pro–Asn–Arg–Phe–Arg–Gly–Lys–Asp–Leu^{22}– segment found in the crystal structure of *Herpes simplex* virus glycoprotein D1 are also given in Table II.[28]

H–Leu^9–Lys–Met–Ala–Asp–Pro–Asn–Arg–Phe–Arg–Gly–Lys–Asp–Leu^{22}–NH$_2$. CYANA calculations for the free peptide H–Leu^9–Lys–Met–Ala–Asp–Pro–Asn–Arg–Phe–Arg–Gly–Lys–Asp–Leu^{22}–NH$_2$ produced a set of conformations with a relatively low target function while no dihedral angle or distance restraint violations were observed (Table I). Ten structures with the lowest energy were selected for further analysis. In the selected structures, the backbone atoms fit with a root mean square displacement (RMSD) of 1.0 Å, while at the segment –Ala^{12}– · · · –Asp^{21}– the RMSD is reduced to 0.32 Å (Table I). This indicates that the backbone of the peptide—except of the N-terminal tripeptide, which exhibits a rather high flexibility—adopts a rather rigid conformation. Moreover, the corresponding RMSD value for the region –Asp^{13}– · · · –Arg^{16}– is only 0.09 Å. This region is characterized by the occurrence of a hydrogen bond (Arg^{16}:HN → Asp^{13}:O) in all 10 best structures (Table III), which stabilizes a type I (III) β-turn. This finding is in agreement with the NMR results. The φ and ψ values of the two central residues are -75 ± 0, $-22 \pm 4°$ for Pro^{14} and -71 ± 0, $-8 \pm 2°$ for Asn^{15}, respectively (Table II). As already mentioned, the difference between the type I and III β-turn is small and refers only to φ and ψ values of the $i + 2$ residue of the turn. Therefore, we can accept that the ψ value of $-8 \pm 2°$ found for Asn^{15} ($i + 2$ residue of the turn) is close to 0 and probably indicates a shifting of the equilibrium toward the type I β-turn. The

Table I Classification of Restraints Used as Input in CYANA Calculations and Statistics of the 10 Lower Target Function Structures of Free Epitope [Nle^{11}]gD-9-22, Ac-[SOC$_4$([Nle^{11}]gD-9-22)$_4$], Ac-[SOC$_4$([Nle^{11}]gD-9-22-Cys)$_4$], and T20 ([Nle^{11}]gD-9-22-Cys)$_4$

	[Nle^{11}] gD-9-22	Ac-[SOC$_4$([Nle^{11}] gD-9-22)$_4$]	Ac-[SOC$_4$([Nle^{11}] gD-9-22-Cys)$_4$]	T20([Nle^{11}] gD-9-22-Cys)$_4$
Restraint Classification				
Number of NOEs	138	94	152	115
Backbone–backbone NOEs	44	33	36	31
Backbone–side-chain NOEs	83	58	99	72
Side-chain–side-chain NOEs	11	3	17	12
Intra residue NOEs	74	53	91	75
Inter residue NOEs	64	41	61	40
Sequential NOEs	38	27	38	36
Short-range NOEs	26	14	23	4
Long-range NOEs	0	0	0	0
Strong NOEs (<2.8 Å)	35	38	34	39
Medium NOEs (<3.5 Å)	60	37	77	57
Weak NOEs (<5 Å)	43	19	41	19
J	11	0	0	0
$^3J_{N\alpha}$	11	0	0	0
Calculation Results				
Number of structures calculated	100	100	100	100
Final structures	10	10	10	10
Min/max target function of final structures	0.10–0.19	0.69–0.69	0.19–0.22	0.12–0.14
Distance restraint violations > 0.3 Å	0	2	0	0
Distance restraint violations > 0.2 Å	0	3	1	0
Torsion angle violations	0	1	0	0
Mean global backbone RMSD	1.00 ± 0.59	1.61 ± 0.69	1.52 ± 0.50	1.53 ± 0.65
Mean global heavy atom RMSD	1.64 ± 0.50	2.10 ± 0.33	2.20 ± 0.50	2.24 ± 0.53
Mean global backbone RMSD (residues 12–21)	0.32 ± 0.07	0.28 ± 0.19	0.49 ± 0.16	0.77 ± 0.39
Mean global heavy atom RMSD (residues 12–21)	1.48 ± 0.37	1.06 ± 0.22	1.44 ± 0.28	1.50 ± 0.44

backbone conformation of the peptide in the segment –Asp^{13}–Pro–Asn–Arg–Phe–Arg–Gly–Lys–Asp^{21}– is stabilized by six ($i + 3 \rightarrow i$) hydrogen bonds, while the φ and ψ dihedral angle values deviate from an ideal 3_{10}-helical structure (Table II, Figure 7A). The Asp^{13}–NH amide proton was found to be involved simultaneously in two hydrogen bonds with Lys^{10}–CO (in all 10 lower target function structures) and Met^{11}–O (in 6 out of the 10 lowest target function structures). Similarly, the Asp^{21}–NH amide proton was found to participate in two hydrogen bonds with Arg^{18}–CO (in all 10 lower target function structures) and Gly^{19}–CO (in all 10 lower target function structures) (Table III). Despite the presence of several opposite charged side chains in the peptide sequence, no hydrogen-bonded side-chain–side-chain interactions were observed. However, the distance between the side-chain charged centers of Asp^{13}/Arg^{16} and of Arg^{18}/Asp^{21} was found in the region of ~6.5–11.0 Å in all 10 lower target function structures. Therefore, ionic interactions could be established that probably favor the 3_{10}-helix stabilization.[38]

H–Leu^9–Lys–Met–Ala–Asp–Pro–Asn–Arg–Phe–Arg–Gly–Lys–Asp–Leu^{22}– conjugated to Ac–(Lys–Aib–Gly)$_4$–OH Carrier. In the selected 10 lowest target function structures, the backbone atoms fit with RMSD of 1.61 ± 0.69 Å, while at the region –Ala^{12}–· · · –Asp^{21}– the RMSD is reduced to 0.28 ± 0.19 Å (Table I). The low RMSD value in the central decapeptide indicates, as in the free epitope, that the backbone adopts a rather rigid conformation. The N-terminal tripeptide conserves its high flexibility despite the conjugation to the carrier. The RMSD value in the region –Asp^{13}– · · · –Arg^{16}– is only 0.09 ± 0.08 Å. The occurrence of the hydrogen bond between Arg^{16}:HN → Asp^{13}:O in all 10 lower target function structures stabilizes a β-turn in this segment (Table III). The φ and ψ values of the two central residues

Table II Backbone Dihedral Angles of the Fragment 9–22 in the Crystal Structure of the *Herpes simplex* Virus Glycoprotein D-1 (PDB code 1jma) and Average Values of the Synthetic Compounds Obtained from NMR Based Structure Calculations

	Protein (X-Ray)		[Nle^{11}]gD-9-22		Ac-[SOC$_4$([Nle^{11}]gD-9-22)$_4$]		Ac-[SOC$_4$([Nle^{11}]gD-9-22-Cys)$_4$]		T20([Nle^{11}]gD-9-22-Cys)$_4$	
Residue[a]	φ	ψ	φ	ψ	φ	ψ	φ	ψ	φ	ψ
Leu^{9}	−62.9	−24.9		136.9 ± 51		101.9 ± 37		136.9 ± 41		23.5 ± 85
Lys^{10}	−61.3	−31.5	−97.8 ± 31	131.2 ± 45	−104.4 ± 27	111.1 ± 42	−81.7 ± 31	121.3 ± 42	−71.2 ± 50	138.8 ± 18
Met/Nle^{11}	−138.2	177.5	−58.5 ± 0	−30.7 ± 15	−146.2 ± 56	166.1 ± 101	−164.8 ± 33	128.7 ± 38	−38.0 ± 1	−42.0 ± 17
Ala^{12}	−50.2	153.5	−111.0 ± 34	44.1 ± 7	−54.8 ± 7	114.4 ± 25	−95.2 ± 61	142.9 ± 32	−133.8 ± 43	48.6 ± 4
Asp^{13}	−70.6	123.4	−78.3 ± 37	162 ± 2	−62.0 ± 15	120.2 ± 15	−63.3 ± 14	129.1 ± 18	−56.4 ± 55	120.3 ± 32
Pro^{14}	−63.4	−17.2	−75.0 ± 0	−22.2 ± 4	−75.0 ± 0	−2.7 ± 0	−75.0 ± 0	−2.6 ± 3	−75.0 ± 0	−9.7 ± 1
Asn^{15}	−103.5	−7.1	−70.6 ± 0	−8.1 ± 2	−74.4 ± 0	−30.5 ± 0	−74.5 ± 0	−19.2 ± 0	−72.3 ± 0	−21.6 ± 0
Arg^{16}	−64.4	−43.4	−60.2 ± 5	−21.2 ± 2	−65.1 ± 0	−12 ± 0	−63.7 ± 0	−8.5 ± 0	−63.2 ± 2	−11.0 ± 1
Phe^{17}	−102	77.1	−67.1 ± 0	−5.7 ± 0	−72.1 ± 0	−40.3 ± 0	−50.2 ± 0	−33.7 ± 0	−106.9 ± 17	−21.0 ± 4
Arg^{18}	−74.7	−174.1	−97.2 ± 0	−34.8 ± 0	−74.0 ± 0	−10.1 ± 0	−69.2 ± 2	−17.9 ± 0	−54.6 ± 5	−91.5 ± 12
Gly^{19}	102.2	118.0	−64.7 ± 0	−22.7 ± 1	−71.0 ± 0	−32.2 ± 0	−64.5 ± 8	−31.9 ± 4	−43.8 ± 3	−33.8 ± 1
Lys^{20}	−65	−25.3	−91.8 ± 0	31.7 ± 0	−54.0 ± 0	−22.6 ± 0	−63.0 ± 3	−18.0 ± 0	−67.2 ± 7	−53.4 ± 1
Asp^{21}	−76.6	−45.2	−81.2 ± 15	127.9 ± 29	−82.9 ± 0	−20.3 ± 0	−74.9 ± 23	−32.5 ± 12	−43.8 ± 2	124.2 ± 16
Leu^{22}	−40.0	120.9	−67.9 ± 11		−40.5 ± 0		−132.2 ± 44		−112.6 ± 65	

[a] Nle^{11} and C-terminal Cys residues in the synthetic compounds were replaced by Met in CYANA calculations.

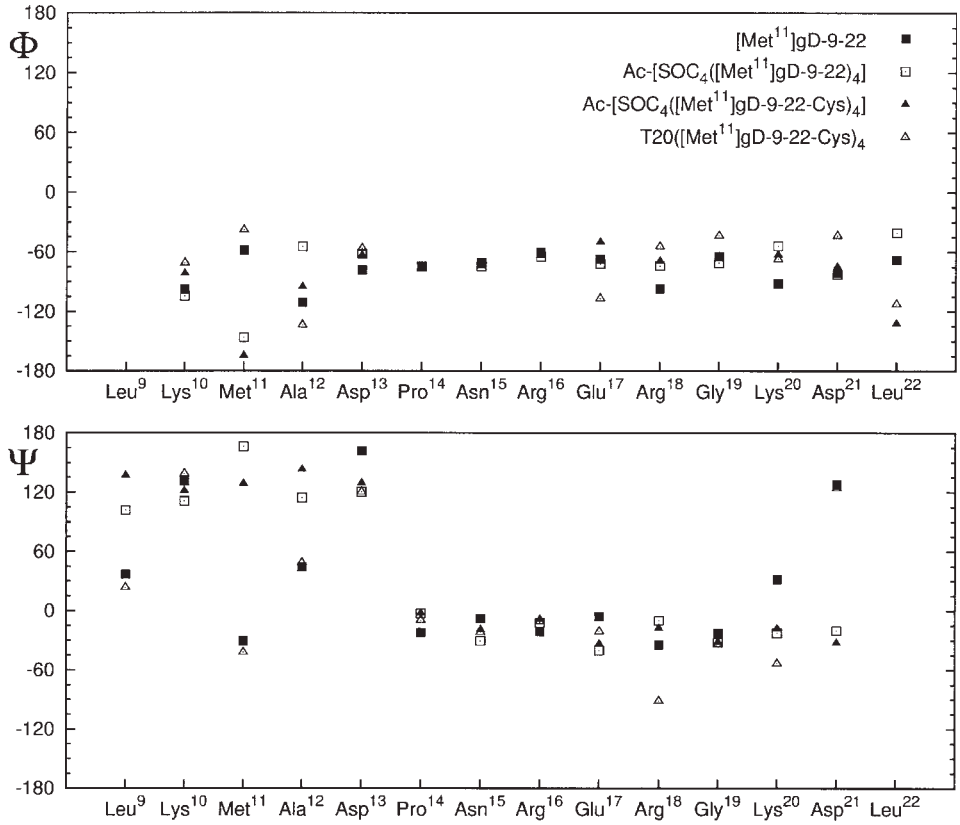

FIGURE 6 Plot of the backbone φ and ψ dihedral angle averaged values of the ten lowest target function structures of the four compounds: free epitope peptide [Nle^{11}]gD-9-22, Ac-[SOC_4([Nle^{11}]gD-9-22)$_4$], Ac-[SOC_4([Nle^{11}]gD-9-22-Cys)$_4$], and T20([Nle^{11}]gD-9-22-Cys)$_4$.

are -75 ± 0 and $-3 \pm 0^\circ$ for P^{14} and -74 ± 0 and $-31 \pm 0^\circ$ for Asn^{15} (Table II), respectively. The φ and ψ angle values of Asn^{15} provide evidence for the presence of type III β-turn. Interestingly, the ψ dihedral angle of Asp^{13} changes from $\sim 162^\circ$ in the free form to $\sim 120^\circ$ in the conjugated form. This change

Table III Hydrogen Bonds Found for the Free and Carrier-Conjugated Epitope Peptide in the 10 Lowest Target Function Structures of CYANA Calculations

Donor	Acceptor[a]	([Nle^{11}] gD-9-22)	Ac-[SOC_4([Nle^{11}] gD-9-22)$_4$]	Ac-[SOC_4([Nle^{11}] gD-9-22-Cys)$_4$]	T20([Nle^{11}] gD-9-22-Cys)$_4$
Asp^{13}:HN	Lys^{10}:O	10	—	—	10
Asp^{13}:HN	Met^{11}:O	6	—	—	4
Arg^{16}:HN	Asp^{13}:O	10	10	10	10
Phe^{17}:HN	Pro^{14}:O	10	10	10	10
Arg^{18}:HN	Asn^{15}:O	10	10	10	10
Gly^{19}:HN	Arg^{16}:O	10	10	10	10
Lys^{20}:HN	Phe^{17}:O	—	10	10	—
Asp^{21}:HN	Arg^{18}:O	10	10	10	8
Asp^{21}:HN	Gly^{19}:O	10	—	—	—
Asp^{21}:HN	Phe^{17}:O	—	—	—	10
Leu^{22}:HN	Gly^{19}:O	—	10	10	—

[a] Nle^{11} and C-terminal Cys residues in the synthetic compounds were replaced by Met in CYANA calculations.

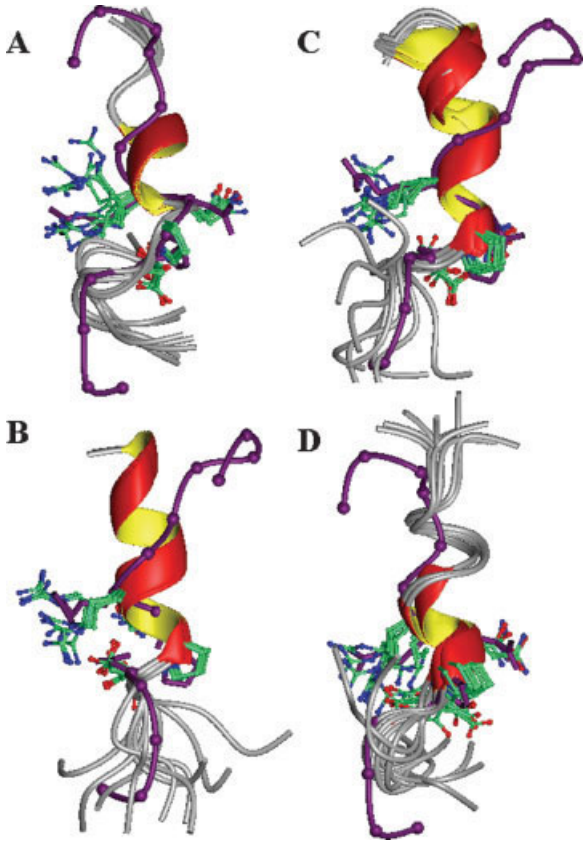

FIGURE 7 Ten lowest target function structures as obtained from NMR-based CYANA calculations. Only the heavy side chain atoms of the region –Asp[13]– · · · –Arg[18]– is shown for clarity of representation. The fragment –Leu[9]– · · · –Leu[22]– of the *Herpes simplex* virus glycoprotein D-1 crystal structure is shown in purple. Free epitope peptide [Nle[11]]gD-9-22 (A), Ac-[SOC_4([Nle[11]]gD-9-22)$_4$] (B), Ac-[SOC_4([Nle[11]]gD-9-22-Cys)$_4$] (C), and T20([Nle[11]]gD-9-22-Cys)$_4$ (D).

alters the relative orientation of the carbonyl group with respect to Asp[13]–C^{α}H and can explain the differences observed for the C^{α}H chemical shift value (Figure 5A). It is worth mentioning that the relative orientation of the side chains of the residues involved in the β-turn structure is quite similar in both the free and conjugated forms (Figure 8). The backbone conformation of the peptide segment –Asp[13]–Pro–Asn–Arg–Phe–Arg–Gly–Lys–Asp[21]– is stabilized by six ($i + 3 \rightarrow i$) hydrogen bonds (Table III), while the φ and ψ dihedral angle values resemble those of a 3_{10}-helical structure (Table II, Figure 7B). In the central part of the conjugated epitope, the φ and ψ angle values are very similar to those found for the free epitope (Figure 6). Some differences occur at the C- and N-terminal segments, which are expected because the N-terminal part of the epitope exhibits a rather high flexibility while the C-terminus is subjected to influences from the carrier.

H–Leu[9]–Lys–Met–Ala–Asp–Pro–Asn–Arg–Phe–Arg–Gly–Lys–Asp–Leu[22]–Met–NH_2 Conjugated to Ac–(Lys–Aib–Gly)$_4$–OH Carrier. The results from the structure calculations of the epitope conjugated through a thioether bond to Ac–(Lys–Aib–Gly)$_4$–OH carrier are almost identical to those found for the epitope conjugated to the same carrier through an amide bond (preceeding case) (Tables II and III, Figures 5B, 6, and 7C). This finding indicates that the type of conjugation does not greatly influence the conformation of the epitope.

H–Leu[9]–Lys–Met–Ala–Asp–Pro–Asn–Arg–Phe–Arg–Gly–Lys–Asp–Leu[22]–Met–NH_2 Conjugated to H–[Thr–Lys–Pro–Lys–Gly]$_4$–NH_2 Carrier. In the selected 10 best structures of H–Leu[9]–Lys–Met–Ala–Asp–Pro–Asn–Arg–Phe–Arg–Gly–Lys–Asp–Leu[22]–Met–NH_2,

FIGURE 8 The lowest target function structures (region –Asp[13]– · · · –Arg[18]–) of the four compounds, superposed to backbone atoms of the corresponding segment of the *Herpes simplex* virus glycoprotein D-1 crystal structure.

when conjugated to tetratuftsin carrier, the backbone atoms fit with a RMSD of 1.53 ± 0.65 Å, while in the region –Ala^{12}– · · · –Asp^{21}– the RMSD is reduced to 0.77 ± 0.39 Å (Table I). This value is higher than that obtained for epitope peptide attached to the SOC_4 carrier. Moreover, the corresponding RMSD value in the region –Asp^{13}– · · · –Arg^{16}– is only 0.22 ± 0.14 Å. Despite the fact that the epitope peptide is attached to a completely different carrier, which adopts a random conformation,[23] the favored conformational characteristics (β-turn) of the epitope are retained. Thus, the hydrogen bond between Arg^{16}–NH and Asp^{13}—CO occurs in all 10 best structures (Table III) and stabilizes a type III β-turn similar to that found for the SOC_4-conjugated epitope. The φ and ψ values of the two central residues are -75 ± 0 and $-10 \pm 1^\circ$ for Pro^{14} and -72 ± 0 and $-21 \pm 0^\circ$ for Asn^{15}, respectively, which are close to values of the type III β-turn. These findings support the NMR results regarding the chemical shift variations observed for the Asn^{15}–NH and Arg^{16}–NH protons in rapport to the free epitope peptide (see also preceding case) (Figure 5C). The ψ dihedral angle of Asp^{13} changes from 162° in the free to ~120° in the T20 carrier-conjugated form, supporting the NMR findings regarding the changes of the Asp^{13}–C$^{\alpha}$H chemical shift (Figure 5C). The backbone conformation of the peptide in the segment –Asp^{13}–Pro–Asn–Arg–Phe–Arg–Gly–Lys–Asp^{21}– is stabilized by four ($i + 3 \rightarrow i$) hydrogen bonds (Table III), in harmony with the higher RMSD value and the lower number of the detected backbone NOE effects compared to the SOC_4-conjugates (Table I, Figure 4D). However, although the C-terminal part of the molecule in this case exhibits a higher mobility compared to the same segment of the epitope in the free form, the N-terminal part seems to possess a better similarity. This is concluded from the fact that the two additional hydrogen bonds of Asp^{13}–NH with Lys^{10}–CO and Met^{11}–CO that were not observed in the SOC_4 conjugates, occur to a similar frequency as that found for the free epitope peptide (Table III).

Comparison of the Epitope Peptide Conformation in Its Free and Conjugated Forms or with Protein ''Built-In'' Crystal Structure. The epitope sequence, –Leu^{9}–Lys–Met–Ala–Asp–Pro–Asn–Arg–Phe–Arg–Gly–Lys–Asp–Leu^{22}–, in the protein crystal structure is characterized by the presence of a type I β-turn in the segment –Asp^{13}–Pro–Asn–Arg^{16}–, while the rest of the sequence adopts an extended conformation.[28] The reported backbone φ and ψ dihedral angle values for the epitope sequence are summarized in Table II. Figure 8 shows the fitting of the lowest target function structures of the four compounds, superposed to the *Herpes simplex* virus glycoprotein gD-1 backbone atoms of the segment –Asp^{13}– · · · –Arg^{16}–. The backbone atoms of the four peptide segments fit to the corresponding sequence of the protein crystal structure with an averaged RMSD value of 0.245 Å, which is very low for structures derived from NMR and crystal structure and refer to different constructs. From the data presented above, it is evident that the β-turn structure of the epitope peptide is present in all forms (free, conjugated, protein built-in) examined in this study. Furthermore, although the conformational equilibrium between types I and III β-turn can be influenced by the state (free or conjugated) of the epitope, the relative orientation of the amino acid side chains of the –Asp^{13}–Pro–Asn–Arg^{16}– segment remains unaffected (Figure 8). This fact could explain the higher antigenicity of the carrier-conjugated epitope because independent of the kind of adsorption (through a copy of the epitope or through the carrier) to ELISA plates several epitope copies, retaining their original activity-determinant conformational features, are available for antibody recognition.

It is expected that the conformation of the epitope peptide segment, adjacent to the site of the conjugation, is influenced by the nature of the carrier and the type of ligation. In agreement with this hypothesis, we observed that attachment to the SOC_4 carrier, with regular secondary structure (distorted 3_{10}-helix), a more ordered conformation at the C-terminal part of the epitope is induced, whereas T20, possessing a random coil structure, has essentially no ordering effect and results in higher C-terminal backbone flexibility. It is therefore of interest to perform similar conformational studies on epitopes that possess the crucial bioactive conformational elements at their C-terminal part.

CONCLUSIONS

In this study we have investigated the effect of artificial carriers on the bioactive conformation of the conjugated epitope peptides. Data obtained and summarized here could contribute to the understanding of the improved antigenic properties of conjugated epitope peptides. The selected *Herpes simplex* virus glycoprotein gD-1 epitope peptide, H–Leu^{9}–Lys–Nle–Ala–Asp–Pro–Asn–Arg–Phe–Arg–Gly–Lys–Asp–Leu^{22}–NH_2, combined with the sequential oligopeptide carriers of different secondary structure permitted a detailed and comparative conformational analysis of the conjugated epitope. Our data published earlier demonstrated that

that conjugates Ac-[SOC_4([Nle^{11}]gD-9-22-Cys)$_4$] and T20([Nle^{11}]gD-9-22-Cys)$_4$ with a thioether bond required roughly the same amount, while for Ac-[SOC_4([Nle^{11}]gD-9-22)$_4$] with amide linkage slightly more was needed in comparative monoclonal antibody binding direct ELISA experiments. The carrier-bound epitope peptides are recognized more efficiently (5–17-fold) than free peptide.[9] In competition ELISA experiments, all three conjugates required similar amounts of peptide, which was approximately five times less than that needed of the nonconjugated peptide [Nle^{11}]gD-9-22 to inhibit the binding of peptide [Nle^{11}]gD-9-22 and Mab A16.[9] These results correlate very well with the findings regarding the activity-determinant secondary conformational elements (β-turn) of the epitope. More precisely, the secondary structure of the glycoprotein gD-1 epitope peptide in its free form is stabilized by a type I/III β-turn in the –Asp^{13}–Pro–Asn–Arg^{16}–, segment with the equilibrium shifted toward type I. The β-turn structure is highly conserved in the conjugated form with the equilibrium shifted toward type III. Moreover, we observed that, in the sequential oligopeptide carrier (SOC_4 and T20) based conjugates, no epitope–epitope or epitope–carrier interactions could be detected. This feature probably allows a better accessibility to the epitope for monoclonal antibody leading to at least enhanced antigenicity. On the other hand, these findings suggest that the sequential oligopeptide carriers might be useful tools for eliciting epitope specific antibodies with high probability to recognize the intact protein. Despite the fact that the C-terminal part of the epitope adopts an extended conformation in the protein crystal structure, in the free form as well as in the conjugated form, helical characteristics are favored in aqueous solution at pH 4.0 and 4°C. No significant differences were observed between thioether or amide bond ligated conjugates of SOC_4 carrier. The C-terminal structure of the epitope upon conjugation can be influenced by the type of sequential oligopeptide carriers because a more ordered conformation was induced by the SOC_4 carrier, which exhibits a regular secondary structure, whereas T20, possessing a random coil structure, results in a higher C-terminal backbone flexibility.

Finally, we have experienced that the conformational features of the epitope peptide conjugated to sequential oligopeptide carriers could be easily estimated by ^{1}H-NMR spectroscopy. This kind of study are facilitated by the fact that epitope–epitope or epitope–carrier interactions are not favored.

These studies were supported by grants from the ''Peptide Based Synthetic Antigens Against Infectious Diseases'' COST Chemistry Action (D13/0007/00) and from Hungarian National Science Fund (OTKA T 043576 and T 049814).

REFERENCES

1. Tam, J. P. Proc Natl Acad Sci USA 1988, 85, 5409–5413.
2. Tam, J. P.; Lu, Y. A. Proc Natl Acad Sci USA 1989, 86, 9084–9088.
3. Tsikaris, V.; Sakarellos, C.; Cung, M. T.; Marraud, M.; Sakarellos-Daitsiotis, M. Biopolymers 1996, 38, 291–293.
4. Tsikaris, V.; Sakarellos, C.; Sakarellos-Daitsiotis, M.; Orlewski, P.; Marraud, M.; Cung, M. T.; Vatzaki, E.; Tzartos, S. Int J Biol Macromol 1996, 19, 195–205.
5. Tsikaris, V.; Sakarellos, C.; Sakarellos-Daitsiotis, M.; Cung, M. T.; Marraud, M.; Konidou, G.; Tzinia, A.; Soteriadou, K. P. Peptide Res 1996, 9, 240–247.
6. Hudecz, F.; Pimm, M. V.; Rajnavölgyi, E.; Mezö, G.; Fabra, A.; Gaál, D.; Kovács, A. L.; Horváth, A.; Szekerke, M. Bioconjugate Chem 1999, 10, 781–790.
7. Mezö, G.; Kajtár, J.; Nagy, I.; Szekerke, M.; Hudecz, F. Biopolymers 1997, 42, 719–730.
8. Hudecz, F. Biologicals 2001, 29, 197–207.
9. Mezö, G.; de Oliveira, E.; Krikorian, D.; Feijlbrief, M.; Jakab, A.; Tsikaris, V.; Sakarellos, C.; Welling-Wester, S.; Andreu, D.; Hudecz, F. Bioconjugate Chem 2003, 14, 1260–1269.
10. Haro, I.; Gömara, M. J. Curr Protein Pept Sci 2004, 5, 425–433.
11. Yiannaki, E. E.; Tzioufas, A. G.; Bachmann, M.; Hantoumi, J.; Tsikaris, V.; Sakarellos-Daitsiotis, M.; Sakarellos, C.; Moutsopoulos, H. M. Clin Exp Immunol 1998, 112, 152–158.
12. Alexopoulos, C.; Tsikaris, V.; Rizou, C.; Panou-Pomonis, E.; Sakarellos-Daitsiotis, M.; Sakarellos, C.; Vlachoyiannopoulos, P. G.; Moutsopoulos, H. M. J Peptide Sci 2001, 7, 105–114.
13. Wilkinson, K. A.; Vordermeier, M. H.; Wilkinson, R.; Iványi, J.; Hudecz, F. Bioconjugate Chem 1998, 9, 539–547.
14. Strongylis, C.; Voidarou, C.; Tsoukatos, D.; Naka, K.; Michalis, L.; Soteriadou, K.; Sakarellos-Daitsiotis, M.; Sakarellos, C.; Tsikaris, V. J Peptide Sci 2004, 10(S2), 293.
15. Tsikaris, V.; Vlachoyiannopoulos, P. G.; Panou-Pomonis, E.; Marraud, M.; Sakarellos, C.; Moutsopoulos, H. M.; Sakarellos-Daitsiotis, M. Int J Peptide Protein Res 1996, 48, 319–327.
16. Sakarellos. C.; Tsikaris, V.; Panou-Pomonis, E.; Alexopoulos, C.; Sakarellos-Daitsiotis, M.; Petrovas, C.; Vlachoyiannopoulos, P. G.; Moutsopoulos, H. M. Lett Peptide Sci 1997, 4, 447–454.
17. Petrovas, C.; Vlachoyiannopoulos, P. G.; Tzioufas, A. G .; Alexopoulos, C.; Tsikaris, V.; Sakarellos-Daitsiotis, M.; Sakarellos, C.; Moutsopoulos, H. M. J Immunol Methods 1998, 220, 59–68.

18. Sakarellos-Daitsiotis, M.; Tsikaris, V.; Sakarellos, C.; Vlachoyiannopoulos, P. G.; Tzioufas, A. G.; Moutsopoulos, H. M. Vaccine 2000, 18, 302–310.
19. Sakarellos-Daitsiotis, M; Tsikaris, V.; Vlachoyiannopoulos, P. G.; Tzioufas, A. G.; Moutsopoulos, H. M.; Sakarellos, C. Methods 1999, 19, 133–141.
20. Keramisanou, D.; Tsikaris, V.; Sakarellos-Daitsiotis, M.; Sakarellos, C.; Mikhailova, A. A.; Strelkov, L. A. J Peptide Res 2002, 60, 178–185.
21. Alexopoulos, C.; Tsikaris, V.; Rizou, C.; Sakarellos-Daitsiotis, M.; Sakarellos, C.; Cung, M. T.; Marraud, M.; Vlachoyiannopoulos, P. G.; Moutsopoulos, H. M. Biopolymers 2000, 54, 1–10.
22. Mezö, G.; Mezö, I.; Pimm, M. V.; Kajtár, J.; Seprödi, A.; Teplán, I.; Kovács, M.; Vincze, B.; Pályi, I.; Idei, M.; Szekerke, M.; Hudecz, F. Bioconjugate Chem 1996, 7, 642–650.
23. Mezö, G.; Kalászi, A.; Reményi, J.; Majer, Z.; Hilbert, Á.; Láng, O.; Köhidai, L.; Barna, K.; Gaál, D.; Hudecz, F. Biopolymers 2004, 73, 645–656.
24. Mezö, G.; Manea, M.; Jakab, A.; Kapuvári, B.; Bösze, S.; Schlosser, G.; Przybylski, M.; Hudecz, F. J Peptide Sci 2004, 10, 701–713.
25. Mezö, G.; Mihala, N.; Andreu, D.; Hudecz, F. Bioconjugate Chem 2000, 11, 484–491.
26. Welling-Wester, S.; Feijlbrief, M.; Koedijk, D. G. A. M.; Drijfhout, J. W.; Weijer, A. J.; Scheffer, A. J.; Welling, G. W. Arch Virol 1994, 138, 331–340.
27. Eisenberg, R. J.; Long, D.; Ponce de Leon, M.; Matthews, J. T.; Spear, P. G.; Gibson, M. G.; Lasky, L. A.; Berman, P.; Golub, E.; Cohen, G. H. J Virol 1985, 53, 634–644.
28. Carfi, A.; Willis, S. H.; Whitbeck, J. C.; Krummenacker, C.; Cohen, G. H.; Eisenberg, R. J.; Wiley, D. C. Mol Cell 2001, 8, 169–179.
29. Kumar, A.; Wagner, G.; Ernst, R. R.; Wüthrich, K. J Am Chem Soc 1981, 103, 3654–3658.
30. Piotto, M.; Saudek, V.; Sklenar, V. J Biomol NMR 1992, 2, 661–665.
31. Sklenar, V.; Piotto, M.; Leppik, R.; Saudek, V. J Magn Reson 1993, 102A, 241–245.
32. Bartels, C.; Xia, T. H.; Billeter, M.; Güntert, P.; Wüthrich, K. J Biomol NMR 1995, 5, 1–10.
33. Heber-Katz, E.; Hollósi, M.; Dietzschold, B.; Hudecz, F.; Fasman, G. D. J Immunol 1985, 135, 1385–1390.
34. Güntert, P.; Mumenthaler, C.; Wüthrich, K. J Mol Biol 1997, 273, 283–298.
35. Herrmann, T.; Guntert, P.; Wuthrich, K. J Mol Biol 2002, 319, 209–227.
36. Koradi, R.; Billeter, M.; Wüthrich, K. J Mol Graphics 1996, 14, 51–55.
37. Wüthrich, K. In NMR of Proteins and Nucleic Acids; John Wiley & Sons: New York, 1986; pp 117–129.
38. Crisma, M.; Formaggio, F.; Moretto, A.; Toniolo, C. Biopolymers (Peptide Sci) 2006, 84, 3–12.
39. Williamson, M. P.; Handa, B. K.; Hall, M. J. Int J Peptide Protein Res 1986, 27, 562–568.
40. Williamson, M. P.; Handa, B. K.; Hall, M. J. Eur J Biochem 1986, 158, 527–536.
41. Sharman, G. J.; Griffiths-Jones, S. R.; Jourdan, M.; Searle, M. S. J Am Chem Soc 2001, 123, 12318–12324.
42. Beger, R. D.; Bolton, P. H. J Biomolecular NMR 1997, 10, 129–142.
43. Möhle, K.; Gussmann, M.; Hofmann, H.-J. J Comput Chem 1997, 18, 1415–1430.
44. Francis, A. K.; Iqbal, M.; Balaram, P. FEBS Lett 1983, 155, 230–232.
45. Sudha, T. S.; Vijayakumar, E. U.; Balaram, P. 1983, J Pept Protein Res 1983, 22, 464–468.